ACS APPLIED MATERIALS & INTERFACES

Research Article

www.acsami.org

# Mesoscopic Simulations of the Phase Behavior of Aqueous $EO_{19}PO_{29}EO_{19}$ Solutions Confined and Sheared by Hydrophobic and Hydrophilic Surfaces

Hongyi Liu,[†,‡] Yan Li,[§] Wendy E. Krause,[†] Melissa A. Pasquinelli,*[,†] and Orlando J. Rojas*[,†,⊥,∥]

[†]Fiber and Polymer Science Program and Department of Textile Engineering, Chemistry and Science and [⊥]Department of Forest Biomaterials, North Carolina State University, Raleigh, North Carolina 27695, United States

[§]The KAUST-Cornell Center for Energy and Sustainability (KAUST-CU), Cornell University, Ithaca, New York 14853, United States

Supporting Information

**ABSTRACT:** The MesoDyn method is used to investigate associative structures in aqueous solution of a nonionic triblock copolymer consisting of poly(propylene oxide) capped on both ends with poly(ethylene oxide) chains. The effect of adsorbing (hydrophobic) and nonadsorbing (hydrophilic) solid surfaces in contact with aqueous solutions of the polymer is elucidated. The macromolecules form self-assembled structures in solution. Confinement under shear forces is investigated in terms of interfacial behavior and association. The formation of micelles under confinement between hydrophilic surfaces occurs faster than in bulk aqueous solution while layered structures assemble when the polymers are confined between hydrophobic surfaces. Micelles are deformed under shear rates of 1 $\mu s^{-1}$ and eventually break to form persistent, adsorbed layered structures. As a result, surface damage under frictional forces is prevented. Overall, this study indicates that aqueous triblock copolymers of poly(ethylene oxide) (PEO) and poly(propylene oxide) (PPO) (Pluronics, $EO_mPO_nEO_m$) act as a boundary lubricant for hydrophobic surfaces but not for hydrophilic ones.

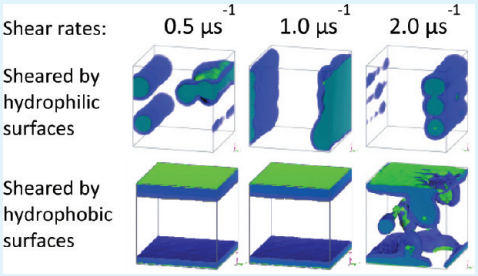


**KEYWORDS:** *triblock nonionic polymers, pluronics, MesoDyn, lubrication, boundary layer, spherical micelles, cylindrical micelles, wormlike micelles*

## INTRODUCTION

Polymers are often used to adjust the functional and interfacial properties of surfaces by adsorption and surface assembly.[1,2] For example, nonionic triblock copolymers comprising ethylene oxide (EO) and propylene oxide (PO) blocks (Pluronics, $EO_mPO_nEO_m$), have received increased attention as a modifier of solid surfaces by physical adsorption.[3−5] One of the advantages of $EO_mPO_nEO_m$ is their amphiphilic properties that endow molecular constructs with tailorable surface affinities,[6] depending on the adsorbing surface and the surrounding medium. For example, these materials are of interest as drug-delivery vehicles because in aqueous solution their micelles contain a hydrophilic corona and a hydrophobic core within which drugs can be solubilized and transported.[7,8] Pluronic triblock copolymers have also been successfully used as surfactants, emulsifiers, stabilizers, and food additives.[7−13]

The interfacial behaviors of $EO_mPO_nEO_m$ solutions in the presence of solid surfaces, both mineral and polymeric, have been investigated by a number of authors.[4,14−26] For example, by using atomic force microscopy, Brandani and Stroeve[24] reported on the formation of a uniform and monolayer-like adsorbed structure of $EO_mPO_nEO_m$ copolymers on hydrophobic surfaces. Rojas and co-workers[4] investigated the adsorption of $EO_{37}PO_{56}EO_{37}$ triblock copolymer on different types of surfaces, namely, polypropylene, poly(ethylene terephthalate), nylon, graphite, cellulose and silica. They found that the hydrophobic mineral surfaces adsorbed molecules of $EO_{37}PO_{56}EO_{37}$ as a monolayer, whereas spherical micellar structures were observed on the hydrophilic ones. Li et al. studied the effect of molecular weight as well as the EO/PO molar ratio on polymer-surface interactions.[27]

A further understanding of the interfacial behaviors and self-assembly processes is required; however, such endeavors are limited by the experimental conditions. Therefore, we utilized mesoscale modeling to provide details about the morphology and dynamics of molecular assemblies of $EO_mPO_nEO_m$ in aqueous solutions and their adsorption on hydrophobic and hydrophilic surfaces. Mesoscopic dynamics (MesoDyn)[28−35] is a simulation method that treats the polymer chains at the coarse-grained level by grouping atoms together up to the equivalent length of the polymers. It is based on the dynamic mean field density functional theory[28,36] in which the phase separation dynamics are described by Langevin-type equations for polymer diffusion and the thermal fluctuation are added as

Received: July 12, 2011
Accepted: December 2, 2011
Published: December 2, 2011

  

**Table 1. Interaction Parameters Used in the MesoDyn Simulations**

| | water (W) | EO (E) | PO (P) | hydrophobic surface (B) | hydrophilic surface (L) |
|---|---|---|---|---|---|
| water (W) | | 1.4 | 5.0 | 5.0 | 0.2 |
| EO (E) | 1.4 | | 4.0 | 1.2 | 0.5 |
| PO (P) | 5.0 | 4.0 | | 0.3 | 3.0 |
| hydrophobicsurface (B) | 5.0 | 1.2 | 0.3 | | |
| hydrophilic surface (L) | 0.2 | 0.5 | 3.0 | | |

noise (random force). A variety of mixed polymer systems have been studied with MesoDyn, such as polyamide 6 with poly(vinyl alcohol), poly(vinyl acetate), and partially hydrolyzed PVAC;[37] poly(vinyl alcohol) with poly(methyl methacrylate);[38] and poly(vinyl pyrrolidone) with poly(bisphenol A-ether sulfone).[39] MesoDyn has also been successfully applied to concentrated aqueous solutions of $EO_mPO_nEO_m$.[35−40]

The focus of our work is on $EO_{19}PO_{29}EO_{19}$, which is an amphiphilic polymer with balanced hydrophilic and hydrophobic segments of moderate molecular length and has been the subject of other MesoDyn simulations.[40,41] Yang et al.[40] compared three series of triblock copolymers with the same size of hydrophilic EO block but various sizes of hydrophobic PO blocks. The size of the PO block was reported to have a significant effect on the morphology of the polymer in solution and the critical micelle concentration (CMC) of $EO_{19}PO_{29}EO_{19}$ at 25 °C was determined by their simulation to be 43%. The effect of shearing forces on the morphology of $EO_{19}PO_{29}EO_{19}$ solutions has been investigated by performing simulations in the absence of external surfaces.[41] It was found that the presence of shearing forces impacted the morphology of $EO_{19}PO_{29}EO_{19}$. Under relative weak shear (1000−2000 $s^{-1}$), distortions of the morphology were observed, and it was suggested that the oscillations in the order parameter indicated the ease to which the morphology could be restored. Under strong shear (>2000 $s^{-1}$) the time taken for new morphologies to form decreased with the shear rate. In addition, the order parameter reached equilibrium rather quickly, indicating that the new morphologies were stable. Finally, it was concluded that block copolymers such as $EO_{19}PO_{29}EO_{19}$ can aggregate more easily (and more stably) when an external force is applied.[41]

Most of the aforementioned studies have addressed the solution behaviors of these polymers and only a few mesoscale simulations have involved assembly and shear effects under confinement between solid surfaces. For example, Knoll and co-workers[42] investigated the morphology of a polystyrene−polybutadiene−polystyrene triblock copolymer in chloroform in contact with polished silicon substrates; they found that the results of their MesoDyn simulation were in good agreement with the experimental observations from scanning force microscopy.[43−45] Unfortunately, to the best of our knowledge, aqueous block copolymer systems confined between polymer surfaces have not been investigated with MesoDyn, probably because of the difficulty in acquiring interaction parameters between the multiple components.

In this work, we study the morphology of $EO_{19}PO_{29}EO_{19}$ in aqueous solutions of various concentrations. Hydrophobic and hydrophilic surfaces are used to confine and shear the $EO_{19}PO_{29}EO_{19}$ molecules. It is hypothesized that the formation of associative structures of $EO_{19}PO_{29}EO_{19}$ can be facilitated by confinement via surface-induced or shearing-induced interactions.

## METHODOLOGY

The mesoscale simulations were done with the MesoDyn software program, which is a module of Materials Studio 4.1 from Accelrys Inc., San Diego, CA.[46] The simulations were performed on a Dell PowerEdge SC1420 server with four Intel Xeon 2.80 GHz processors, 4 GB of RAM, Radeon X1300/X1550 Series graphics card, and running Windows 2003 Server.

**MesoDyn.** MesoDyn is based on the principle that the free energy of an inhomogeneous fluid is a function of the local density function, and therefore all thermodynamic functions can be derived.[28,32,35,36] The starting point involves Gaussian chains, which are coarse-grained "spring-and-bead" models for the molecules where the beads are connected in a chain using harmonic oscillator potentials, and all other interactions are described using a mean field potential from density functional theory. The time evolution is described using Langevin dynamics for polymer diffusion. Thermal fluctuations are introduced via "noise" that is dictated by the fluctuation−dissipation theorem. With this model, diffusive and hydrodynamic phenomena in phase-separation dynamics are conserved.[36] As a mean field model, the values selected for the parameters drive the simulation, and thus any polymer surfactant solution with the same set of parameters will behave in the exact same way.

**Gaussian Chain Topology.** The Gaussian chain topology depends on the degree of coarseness of the system. Two factors are crucial to developing the Gaussian chain model: the chain length and the bead size. The squared end-to-end distance of the Gaussian chain must correspond to the length of the atomistic chain, called the equivalent chain method,[47] where a specific characteristic length is defined that is related to the Gaussian chain length of the molecular component, similar to the Kuhn length.[34] Each bead is the same size, and represents a segment of the chain up to the polymer persistence length. The system of interest in these studies, $EO_{19}PO_{29}EO_{19}$ is a polymer with 50/50 weight ratio of PO and EO segments. The Gaussian chain can be represented by $E_4P_9E_4$, which was developed by Yang and co-workers.[40] This Gaussian chain means that four beads of type "E" will represent the 19 units of EO, and nine beads of type "P" will represent the 29 units of PO. In addition, there will be beads of type "W" to represent water.

**Interaction Parameters between EO, PO, and Water.** Another important parameter in MesoDyn is the mean field interaction energy among chemical entities, which quantify characteristics such as hydrophobicity. The interaction parameter represents the pairwise interactions of beads, similar to the $\chi$ parameter defined in the Flory−Huggins model. In the aqueous $EO_{19}PO_{29}EO_{19}$ system, three parameters are needed: the E−P interaction ($\chi_{EP}$), representing EO−PO; the E−W interaction ($\chi_{EW}$), representing EO−water; and the P−W interaction ($\chi_{PW}$), representing PO−water. Fraaije and co-workers[35] indicated that EO homopolymer is a unique one because it is soluble in water even though it is a member of an insoluble homologous series. Estimation of the interaction parameters from first principles is a challenge for these systems because of the strong influence of hydrogen bonding as a result of the competition between water−water and EO-water nonbonds.[48] Note that these parameters can be sensitive to the conditions, such as the temperature and the concentration, particularly for $EO_mPO_nEO_m$ triblock copolymer systems.[40]

The values of interaction parameters from both simulations and experiments vary greatly in the literature.[31,34−36,47] For various chemical compositions of $EO_mPO_nEO_m$ triblock copolymers, the $\chi_{EW}$ values reported varied between 0.3 and 3.3, $\chi_{PW}$ values are

between 1.64 and 4.1, and $\chi_{EP}$ values varied between 3.0 and 7.3, although $\chi_{EP}$ has been estimated to be between 3 and 5 using group contribution methods.[36,40,47,49,50] For example, Yang and co-workers[40] used the interaction parameters adopted by others ($\chi_{EW}$ = 1.4, $\chi_{PW}$ = 1.7, $\chi_{EP}$ = 3.0) to study the morphology of P65, P84, and P103. However, for P65 ($EO_{19}PO_{29}EO_{19}$), they did not observe the formation of micelle structures until the concentration was increased to 43% v/v, a much larger concentration than the experimental value of 4% w/v (30 °C) reported by Alexandridis et al.[51]

The values of the interaction parameters that were used in this study are summarized in Table 1. The interaction parameters were adjusted in order to match the experimentally reported CMC as best as possible under the conditions of interest, noting that previous work[31,36,40,50] concluded that the experimental data were unreliable for EO-PO pairs ($\chi_{EP}$). The interaction parameters of EO-water and PO-EO were set to $\chi_{EW}$ = 1.4 and $\chi_{EP}$ = 4.0, respectively, which corresponds to those used by Li and co-workers.[47]

**Interactions in the Presence of Hydrophobic and Hydrophilic Solid Surfaces.** To create a confined liquid between two solid layers in the MesoDyn model, the interaction parameters between the solid and each component in the simulation lattice must be determined. However, the interaction parameters between the surfaces and the polymers are difficult to obtain due to the cross interactions between the multiple components. Recently, we have reported on the calculation of the interaction energies in aqueous media between poly(alkylene glycol) block copolymers and polypropylene and cellulose surfaces by using molecular dynamics simulation.[52]

We considered two types of surfaces, a hydrophilic one (labeled "L"), comparable to cellulose; and a hydrophobic one (labeled "B"), comparable to PP. We assumed that the strongest attractions in this system were those between water and the hydrophilic surface and with EO units ($\chi_{WL}$ and $\chi_{EL}$, respectively) as well as between PO and the hydrophobic surface ($\chi_{PB}$). In contrast, the strongest repulsions in the system were assumed to be those between water and PO and water and the hydrophobic surface ($\chi_{WP}$ and $\chi_{WB}$, respectively), followed by the interaction between EO and PO and between PO and the hydrophilic surface ($\chi_{EP}$ and $\chi_{PL}$, respectively). Moderate repulsions are expected between EO and both the hydrophobic surface and water ($\chi_{EB}$ and $\chi_{EW}$, respectively). In summary, the interaction parameters for both surfaces were set to the values given in Table 1 based on the previous assumptions and using values provided in previous publications.[28,40,49,50]

**MesoDyn Simulation Conditions.** For all simulations, the following parameters were used: temperature of 25 °C, time step of 50 ns,[31,53] noise scaling parameter of 100,[31,47,49] compressibility parameter of 10,[31,53] grid parameter of 1.1543,[31,36] and bead diffusion coefficient of $1.0 \times 10^{-7}$ $cm^2/s$.[34] The dimension of the simulation lattice was set to 32 × 32 × 32 nm. Three volume concentrations were considered: 10, 25, and 50%. However, only the 10% concentration was used in studies with confined hydrophobic and hydrophilic surfaces to study the impact of shearing on the formation of micellar structures. The MesoDyn models were run for 20 000 steps of dynamics, for a total simulation time of 1000 $\mu$s. When a pair of surfaces was used to confine the simulation lattice at the top and bottom, the solid wall was virtually set on both sides. 10000 steps of shear (500 $\mu$s) were performed at various shear rates (0.5, 1.0, and 2.0 $\mu s^{-1}$) and starting from the previous time point of 1000 $\mu$s.

**Morphology Analysis.** In dynamic simulation processes, an order parameter can be monitored to indicate the changes occurring in the molecular structures, and can thus yield characteristics of the phase separation and compressibility. The order parameter ($P$), which is the mean squared deviation from homogeneity for a particular species (A) in volume $V$, is defined as[40]

$$P_A = \langle(\eta_A - \eta_A^0)^2\rangle \quad (1)$$

where $\eta_A^o$ is the overall volume fraction of species A, and $\eta_A$ is the local volume fraction of species A; note that both quantities are dimensionless in Mesodyn. Therefore, small values for $P_A$ indicate a homogeneous system, and large values suggest strong phase separation.

In addition, the aggregation number ($N$) for the PO blocks can be estimated by

$$N = \frac{4\pi R_c^3}{3nV} \quad (2)$$

where $n$ denotes the number of repeat units, which is 29 for PO in the present case; $R_c$ is the average core radius of the aggregate, which is an output quantity from Mesodyn, and $V$ is the volume of the PO monomer, which was reported by Zhang and co-workers[41] to be about 95.4 $Å^3$.

The free energy of the system can be obtained from MesoDyn including both harmonic potentials for the intra molecular interactions (i.e., Gaussian chain) and a mean field potential for all other interactions. Therefore, the total free energy is defined as

$$F[\rho] = F^{id}[\rho] + F^{mf}[\rho] \quad (3)$$

where $F^{id}$ is the ideal intramolecular free energy and $F^{mf}$ is the free energy of a mean field potential. Details of both free energy terms are discussed in more detail in refs 28, 35, and 36.

## RESULTS AND DISCUSSION

$EO_{19}PO_{29}EO_{19}$ is a symmetric triblock copolymer with a smaller molecular mass compared to other common types, for example $EO_{26}PO_{40}EO_{26}$ and $EO_{37}PO_{58}EO_{37}$. For $EO_{19}PO_{29}EO_{19}$, the PO blocks comprise 50% of the weight segment of the molecule; therefore, smaller associative structures are expected, which could be useful in narrow drug-delivering channels.

**Preliminary Test: Aqueous Solution Phase Behavior of Aqueous $EO_{19}PO_{29}EO_{19}$ in Bulk Solution.** Simulations were performed in water at concentrations by volume of 10, 25, and 50%, which are commonly used in experimental work.[51] The results of these simulations are given in the Supporting Information. As indicated in Figure S1a, the associative structures for $EO_{19}PO_{29}EO_{19}$ in a 10% aqueous solution were spherical micelles, where the PO blocks aggregated in the core of the micelles (Figure S1c) as PO is a relatively more hydrophobic component that minimizes contact with water. The more hydrophilic EO blocks remained in the periphery (Figure S1b) forming the shell of the spherical aggregate that was surrounded by water. As the polymer concentration increased, the morphology changed from micelles to structures of lower average curvature. The morphology of a 25% aqueous $EO_{19}PO_{29}EO_{19}$ solution (Figure S1b) indicates a more complex association at this higher concentration. The PO blocks were still in the core, which built up continuous, wormlike associative structures, but the shape of the PO and EO phases appeared spindlelike. These morphological features are similar to those reported in other simulation work involving a 30% $EO_{19}PO_{29}EO_{19}$ solution.[40] The larger number of $EO_{19}PO_{29}EO_{19}$ chains present when the concentration was increased to 50% contributed to the formation of more compact wormlike micelles (Figure S1c in the Supporting Information). This morphology may have been induced by the high concentration, which increased the contact between molecules and thus larger amounts of wormlike micelles were assembled.

**Morphology of Aqueous Solutions of $EO_{19}PO_{29}EO_{19}$ under Confinement between Hydrophilic Surfaces.** The time evolution of the morphology of a 10% v/v $EO_{19}PO_{29}EO_{19}$ aqueous solution confined between a 32 nm hydrophilic surface at the top and bottom of the simulation lattice is given in Figure


dx.doi.org/10.1021/am200917h | ACS Appl. Mater. Interfaces 2012, 4, 87–95

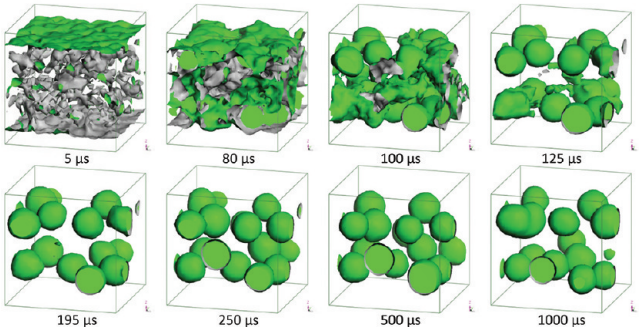


**Figure 1.** Time evolution of PO chains morphology in aqueous 10% v/v $EO_{19}PO_{29}EO_{19}$ solution confined between hydrophilic surfaces (top and bottom, not shown). The simulation time is indicated in each snapshot: 5, 80, 100, 125, 195, 250, 500, and 1000 $\mu$s. Only the PO phase is displayed for clarity.

1. At 5 $\mu$s, the PO phase was randomly distributed in the middle of the confined lattice. Comparing this morphology to the unconfined one at the same simulation time in Figure S2 in the Supporting Information suggests that in the thin slices (3–5 nm) of the solution near the hydrophilic surfaces, there was not a continuous water phase but rather a PO layer. The PO segments started to aggregate and formed large blocks by 80 $\mu$s, resulting in micelles. The formation of micelles was completed by 195 $\mu$s; note that micelle formation was faster (almost by 100 $\mu$s) under these confinement conditions than what was observed in unconstrained systems (see Figure S2 in the Supporting Information). Thereafter, the micelles were stable in the solution and located themselves away from the hydrophilic surface. The micelles tended to form two layers, and these layers seemed to persist with time. This morphology may be due to a reduction in the random-walk space of the hydrophobic PO segments in solution because of the confinement by the parallel hydrophilic surfaces. Interestingly, two micelles merged into one at 1000 $\mu$s; micellar clusters such as this one were also seen by Yang and co-workers[40] for P84 and P103, which can be stable and also concentration-dependent.

The order parameters calculated from eq 1 as a function of the simulation time for the 10% v/v $EO_{19}PO_{29}EO_{19}$ when confined between the hydrophilic surfaces are given in Figure

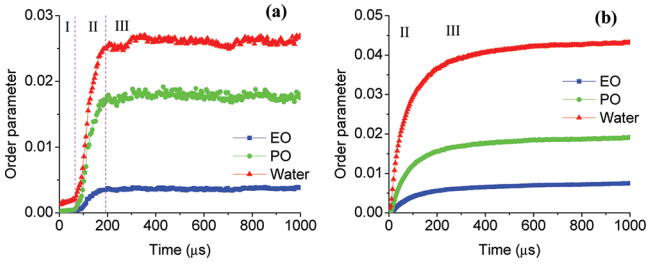


**Figure 2.** Order parameter versus simulation the time for aqueous $EO_{19}PO_{29}EO_{19}$ solution confined by (a) hydrophilic and (b) hydrophobic surfaces. The dashed lines indicate the transitions between phases.

2a. The trend observed is similar to what was observed for the bulk solution with three stages (Figures S1–S2 of Supporting Information document) but with transitions at different simulation time: (I) 0 to 80 $\mu$s; (II) 80 to 195 $\mu$s, and (III) 195 to 1000 $\mu$s. The corresponding snapshots from Figure 1 suggests that the PO phase was randomly confined in stage I. Formation of micelles occurred mainly in stage II; however, this stage took place at shorter times compared to those observed for the bulk solution (see Figure S3a in the Supporting Information). Therefore, the confinement between hydrophilic surfaces may trigger association or formation of micelles.

**Morphology of Aqueous Solutions of $EO_{19}PO_{29}EO_{19}$ under Confinement between Hydrophobic Surfaces.** The time evolution of the morphology of 10% $EO_{19}PO_{29}EO_{19}$ solution confined between parallel hydrophobic surfaces is given in Figure 3. Compared to the previous case of hydrophilic

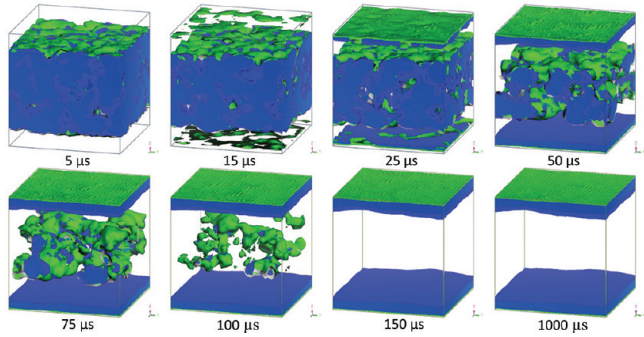


**Figure 3.** Time evolution of PO/EO morphology in aqueous 10% v/v $EO_{19}PO_{29}EO_{19}$ solution confined between hydrophobic surfaces (top and bottom, not shown). The simulation time is indicated in each snapshot: 5, 15, 25, 50, 75, 100, 150, and 1000 $\mu$s. The water phase is removed for clarity. PO chains are shown in green and EO ones in blue.

surfaces, the presence of hydrophobic surfaces produced a completely different morphology profile at the same concentration. At 5 $\mu$s, no continuous phase of $EO_{19}PO_{29}EO_{19}$ was observed on the hydrophobic surfaces, as was observed for the hydrophilic surfaces (Figure 1). As time progresses, however, a lamellar phase began to form on the hydrophobic surfaces, starting at 15 $\mu$s, and phase separation between PO and EO occurred in solution. From 25 to 150 $\mu$s, the thickness of the $EO_{19}PO_{29}EO_{19}$ layers on the hydrophobic surfaces increased until there was no longer a continuous polymer phase in the center of the confined space. After 150 $\mu$s, $EO_{19}PO_{29}EO_{19}$ was completely separated into two layers in the lattice, where the PO segments adhered to hydrophobic surfaces and formed a continuous layer. The EO segments formed the other layer covering in contact with the aqueous phase. The thickness of each layer was approximately 4 nm.

The time evolution of the order parameters of the 10% $EO_{19}PO_{29}EO_{19}$ solution confined between hydrophobic surfaces is given in Figure 2b. In contrast to the unconfined system and the system confined between two hydrophilic surfaces, no stage I was evident, indicating that the polymer aggregation likely occurred extremely rapidly at the beginning of the simulation due to the hydrophobic nature of the surfaces. In addition, no difference or transition between stages II and III were observed, which is likely due to the gradual formation of PO/EO layers rather than other morphologies such as spherical or wormlike micelles.

**Hydrophilic Surfaces under Shear Lubricated by Aqueous $EO_{19}PO_{29}EO_{19}$ Solution.** As was discussed in the previous sections, $EO_{19}PO_{29}EO_{19}$ micelles were self-assembled in the absence of external forces either in an unconfined lattice or under confinement between hydrophilic surfaces (not


dx.doi.org/10.1021/am200917h | ACS Appl. Mater. Interfaces 2012, 4, 87–95

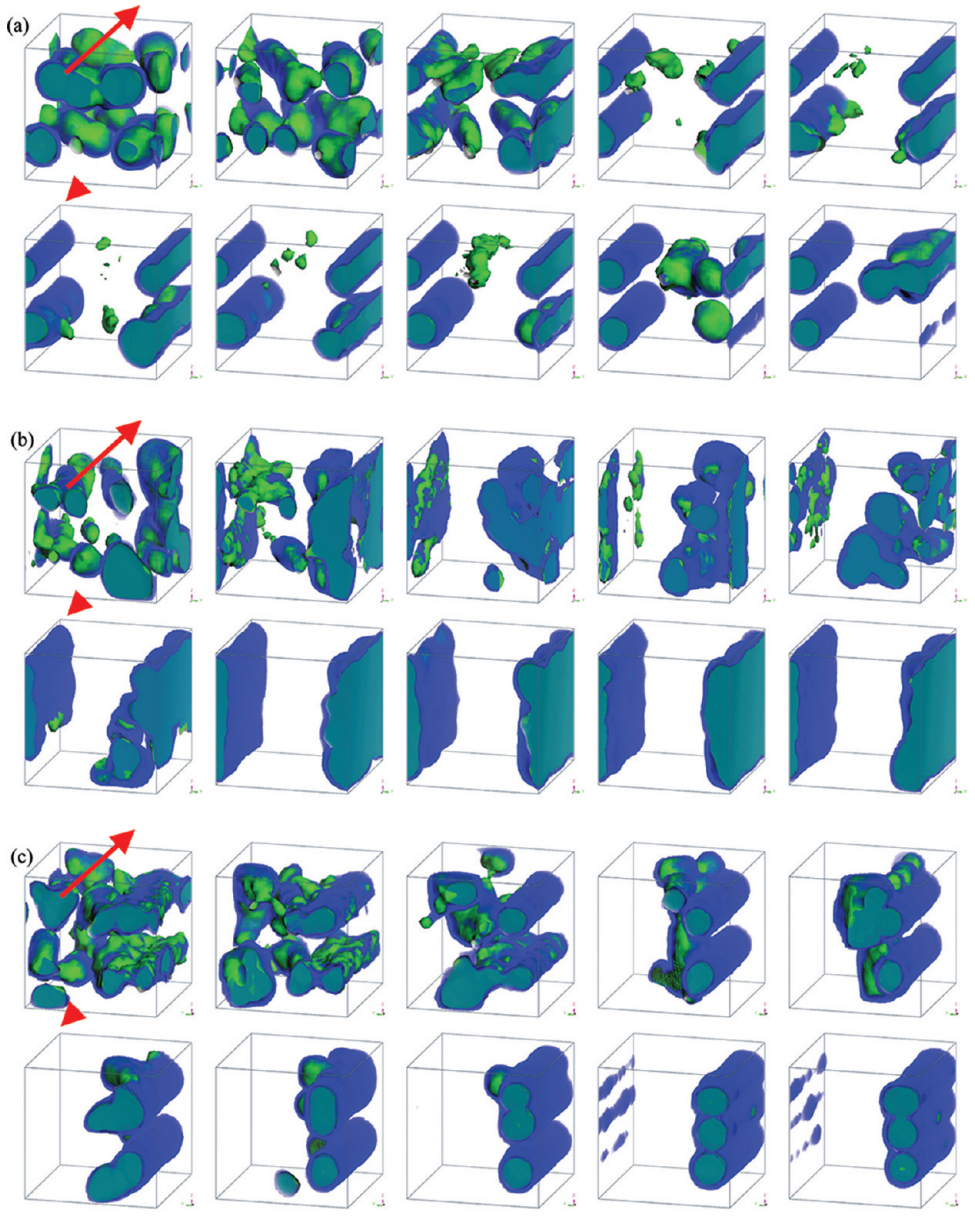


**Figure 4.** Morphology of structures formed from aqueous 10% v/v $EO_{19}PO_{29}EO_{19}$ solution sheared between hydrophilic surfaces as a function of time under various shear rates: (a) 0.5, (b) 1.0, and (c) 2.0 $\mu s^{-1}$, starting from the previous time point, 1000 $\mu s$ simulation time is indicated in Figure 2. The corresponding times from the upper left to the lower right in each subfigure are: 1005, 1010, 1025, 1050, 1100, 1150, 1200, 1250, 1375, and 1500 $\mu s$. The water phase is removed for clarity. PO is indicated with green color and EO is in blue. The red arrows denote the relative direction of shearing for the top and bottom surfaces.

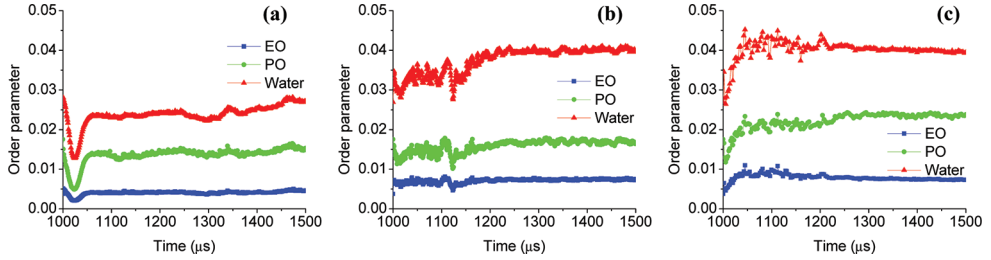


**Figure 5.** Order parameter as a function of simulation time for 10% $EO_{19}PO_{29}EO_{19}$ solution sheared between hydrophilic surfaces with various shear rates: (a) 0.5, (b) 1.0, and (c) 2.0 $\mu s^{-1}$, starting from the previous time point, 1000 $\mu s$ simulation time is indicated in Figure 2.

between hydrophobic surfaces). In order to better understand implications in boundary layer phenomena, an external shearing force was applied. The top and bottom surfaces (either hydrophobic or hydrophilic) were moved in opposite directions relative to each other at (moderate) shear rates of 0.5, 1.0, or 2.0 $\mu s^{-1}$. The final frames generated in the simulation under no


dx.doi.org/10.1021/am200917h | ACS Appl. Mater. Interfaces 2012, 4, 87–95

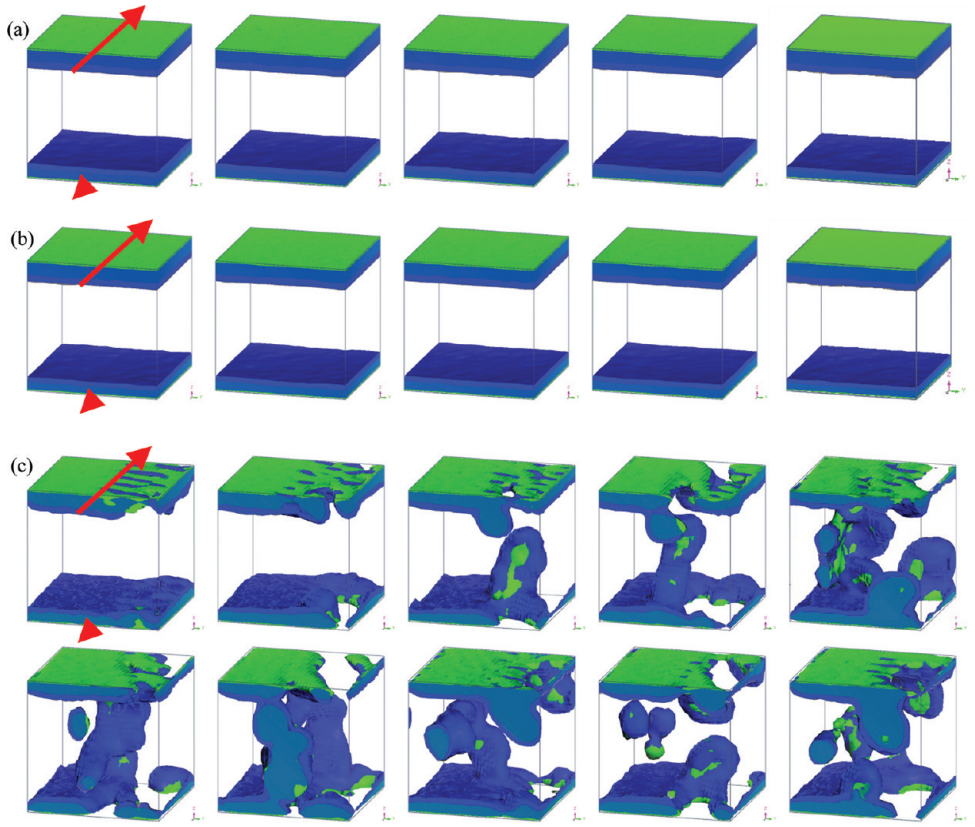


**Figure 6.** Morphology of structures formed from aqueous 10% v/v $EO_{19}PO_{29}EO_{19}$ solution sheared between hydrophobic surfaces as a function of the simulation time under various shear rates: (a) 0.5, (b) 1.0, and (c) 2.0 $\mu s^{-1}$, starting from the previous time point, 1000 $\mu s$. The corresponding times for (a) and (b) from the left to the right are: 1005, 1050, 1125, 1250, and 1500 $\mu s$, while the corresponding times for (c) from the upper left to the lower right are: 1005, 1010, 1025, 1050, 1100, 1150, 1200, 1250, 1375, and 1500 $\mu s$. The water phase is removed for clarity. PO is indicated with green color and EO is in blue. The red arrows denote the relative direction of shearing for the top and bottom surfaces.

shear (previous sections) were used as an initial condition in the present study dealing with shear modes. The morphology as a function of simulation time of 10% v/v aqueous $EO_{19}PO_{29}EO_{19}$ solution sheared between two hydrophilic surfaces is given in Figure 4 in which the empty space in the lattice corresponds to water. The corresponsive plots of the order parameter are given in Figure 5.

Under the shear rate of 0.5 $\mu s^{-1}$, micelles that originally formed between two hydrophilic surfaces in the absence of shear (Figure 1) became distorted at 1005 $\mu s$ as indicated in Figure 4a. From 1005 to 1025 $\mu s$, the phase shape of PO and EO was more and more irregular and the order parameter in Figure 8a dropped significantly. The minimum of the order parameter was at about 1025 $\mu s$, which indicates a relatively disordered morphology. At 1050 $\mu s$, two cylinders with a PO core and EO shell were constructed, while a small part of $EO_{19}PO_{29}EO_{19}$ was outside of these cylinder structures and the PO core exposed to water. From 1050 to 1250 $\mu s$, both cylinders kept a relative stable structure and the order parameter also remained in a small range (Figure 5a). The part of PO and EO that were not part of the cylinder structures became a large conglomeration and the EO was separated to cover the PO core at 1375 $\mu s$, while the order parameter increased to a small peak. At 1500 $\mu s$, the part of EO and PO previously out of the cylinder structures merged with one cylinder, and finally a hybrid conglomeration and a cylinder persisted under a relatively low shear rate of 0.5 $\mu s^{-1}$.

Under the shear rate of 1.0 $\mu s^{-1}$, at the time of 1005 $\mu s$, micelles were distorted. Figure 5b, corresponding to the order parameter for similar conditions, suggests that there was a rapid decrease in order at the beginning of the shearing process, likely due to the distortion. By 1050 $\mu s$, irregular wormlike micelles were formed, and then they began to break up rapidly. Both PO and EO segments tended to aggregate to form large blocks as time increased from 1050 to 1100 $\mu s$. There was a dramatic drop in the order parameters (Figure 5b) as the simulation time increased from 1115 to 1125 $\mu s$. Figure 4b indicates that a new morphology was formed in the lattice, an adsorbed "wall-like" structure. The order parameter was found to increase after 1125 $\mu s$, and there were still some micelle-like structures surrounding the adsorbed chains. Additionally, the PO cores became exposed to water under shear. By 1150 $\mu s$, all $EO_{19}PO_{29}EO_{19}$ molecules are observed to merge into the wall-like structure. During the time span from 1150 to 1500 $\mu s$, the wall-like structure grew thinner perpendicular to the hydrophilic layers, but stretched from the top to the bottom of the lattice and between the hydrophilic surface layers.

Under the shear rate of 2.0 $\mu s^{-1}$, the micellar structures were dramatically destroyed at 1005 $\mu s$ (Figure 4c). Even the order parameter, which did not drop when micelles were broken by other low shear rates, increased sharply at the beginning of the strong shear performance (see Figure 5c). One cylinder was formed at 1025 $\mu s$ and two cylinders were formed by 1050 $\mu s$. From 1050 to 1200 $\mu s$, the order parameter vibrated at a high value range, 0.038−0.045 (Figure 5c), and all EO and PO were


dx.doi.org/10.1021/am200917h | ACS Appl. Mater. Interfaces 2012, 4, 87−95

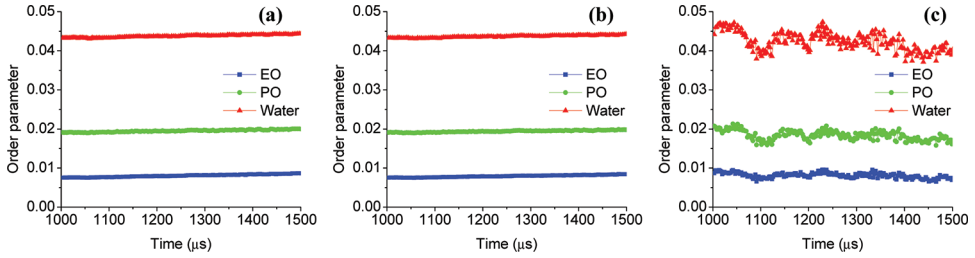


**Figure 7.** Order parameter as a function of the simulation time for 10% $EO_{19}PO_{29}EO_{19}$ solution sheared between hydrophobic surfaces with various shear rates: (a) 0.5, (b) 1.0, and (c) 2.0 $\mu s^{-1}$, starting from the previous time point, 1000 $\mu s$.

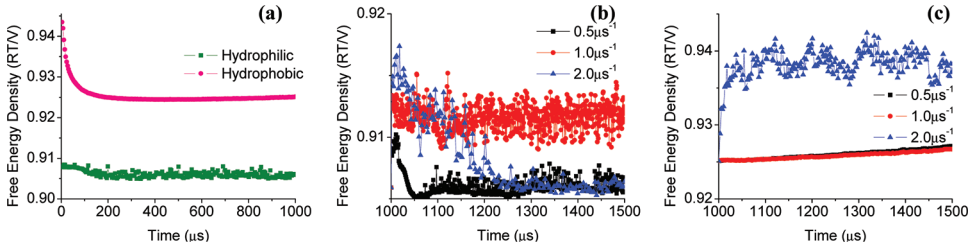


**Figure 8.** Free energy density versus the simulation time for aqueous $EO_{19}PO_{29}EO_{19}$ solution (a) confined by hydrophilic and hydrophobic surfaces, and sheared at various shear rates, 0.5, 1.0, and 2.0 $\mu s^{-1}$ by (b) hydrophilic surfaces and (c) hydrophobic surfaces.

in aggregation with two cylinders as the main body. From 1250 to 1500 $\mu s$, three cylinders were constructed in the direction vertical to the surfaces (Figure 4c) while the order parameter remained level (Figure 5c).

Comparing the results with the three shear rates, the order parameter of PO is higher when the shear rate is higher. Interestingly, there appears to be no contact between the hydrophilic surfaces and this wall-like structure. Therefore, weak adsorption of the $EO_{19}PO_{29}EO_{19}$ occurred on the hydrophilic surfaces, which is in agreement with QCM and AFM measurements reported earlier by us.[4]

**Hydrophobic Surfaces under Shear Lubricated by Aqueous $EO_{19}PO_{29}EO_{19}$.** Snapshots of the morphology of 10% v/v aqueous $EO_{19}PO_{29}EO_{19}$ solution sheared between hydrophobic surfaces as a function of the simulation time at the constant shear rates of 0.5, 1.0, or 2.0 $\mu s^{-1}$ is given in Figure 6. The initial configuration in these shearing simulations was taken from the final frame at 1000 $\mu s$ from the unsheared simulations (Figure 3), where the $EO_{19}PO_{29}EO_{19}$ molecules formed phase-separated layers fully covering the two parallel hydrophobic surfaces with a thickness on the order of 3−4 nm. No significant change in morphology was observed under the shear rates of 0.5 or 1.0 $\mu s^{-1}$ as observed in Figures 6a and 7b, respectively, indicating a strong interaction between the PO chains and the surface. The interaction was high enough to withstand the applied shear field, which was also discovered experimentally.[4] The corresponding order parameter, shown in panels a and b in Figure 7, increased linearly as a function time for the three components in systems under shear, but these changes were quite small and were likely the result of the nonequilibrium nature of the process. Overall, the observations suggest that under shear, the polymer molecules slowly organized into layers and underwent significant changes in their assembly. Therefore, it is expected that $EO_{19}PO_{29}EO_{19}$ is a suitable lubricant for hydrophobic surfaces due to the thin, protecting layer that assembles at the interface in boundary lubrication.

When the shear rate increased to 2.0 $\mu s^{-1}$ in Figure 6c, surprisingly a desorption process was observed from hydrophobic surfaces for 10% v/v aqueous $EO_{19}PO_{29}EO_{19}$ solution. At 1005 $\mu s$, the layer structures of the $EO_{19}PO_{29}EO_{19}$ became uniform and the EO (blue) stripes invaded the PO layer, resulting in the molecules sticking to hydrophobic surfaces due to the high shear rate. At 1010 $\mu s$, several small portions of the adsorbed $EO_{19}PO_{29}EO_{19}$ layers were peeled off and hence an empty patch was promoted on the hydrophobic surface. With an increase in simulation time, more $EO_{19}PO_{29}EO_{19}$ molecules were desorbed from the surface. From 1025 to 1500 $\mu s$, the desorption observed in the morphology was also found to be associated with a disordering process. Figure 7c indicates that the corresponding order parameters of three components in the system changed in an oscillating fashion in the range of simulation time, also suggesting that the system was a dynamical equilibrium state. The desorption and disorder phenomena at high shear rate (2.0 $\mu s^{-1}$) suggests that the hydrophobic surfaces were not able to maintain the adsorbed $EO_{19}PO_{29}EO_{19}$ layer structures because of the high hydrodynamic force promoted by the high shear rate.

**Thermodynamic Free Energy Density Analysis for Aqueous $EO_{19}PO_{29}EO_{19}$ Solution Confined and Sheared by Hydrophilic or Hydrophobic Surfaces.** Figure 8a provides the thermodynamic free energy density of the $EO_{19}PO_{29}EO_{19}$ solution confined by hydrophilic or hydrophobic surfaces. Both of the free energy curves decreased with the simulation time from 0 to 200 $\mu s$, which indicated that the process proceeds spontaneously in the forward direction. The free energy of the system confined by hydrophobic surfaces is as smooth as the order parameter in Figure 2b, whereas the curve of hydrophilic surfaces dropped from 80 to 200 $\mu s$, corresponding to the same range of order parameters in Figure 2a.

For the shear models with hydrophilic surfaces, the free energy density given in Figure 8b decreased with the simulation time in the ranges of 1000−1050 $\mu s$ at the shear rate of 0.5 $\mu s^{-1}$ and within 1000−1250 $\mu s$ at the shear rate of 2.0 $\mu s^{-1}$, but oscillates in a box at the shear rate of 1.0 $\mu s$. The free energy curves also indicated that the cylinder structure is more stable than the wall-like structure. For the shear models with


dx.doi.org/10.1021/am200917h | ACS Appl. Mater. Interfaces 2012, 4, 87−95

hydrophobic surfaces, all three curves of free energy at various shear rates generally increased with the simulation time, which indicated that the process proceeds spontaneously in reverse. If the shear action ceased, the morphology of the aqueous $EO_{19}PO_{29}EO_{19}$ solution would turn back to the same at 1000 $\mu$s. The weak shear rates of 0.5 and 1.0 $\mu s^{-1}$ slightly increased the free energy by peeling some individual molecules from the absorbed surfaces, but these molecules hardly changed the morphology of the solution. Under the strong shear rate of 2.0 $\mu s^{-1}$, the free energy increased dramatically at the beginning of shear performance when the adsorbing polymer layers were disordered by the hydrodynamic force induced by a high shear rate.

## CONCLUSIONS

A symmetric nonionic triblock copolymer, $EO_{19}PO_{29}EO_{19}$, was found to form unique self-assembled structures in aqueous solution, depending on the polymer concentration. Compared to the case of bulk solution, $EO_{19}PO_{29}EO_{19}$ confined between two hydrophilic surfaces associated at a faster rate and formed structures that were repelled away from the interface. Under a shear rate of 1 $\mu s^{-1}$, micelles were distorted and aggregated into a wall-like structure, avoiding contact with the surface. The order parameter confirmed the dynamics of this process. $EO_{19}PO_{29}EO_{19}$ was therefore suggested as poor lubricant for hydrophilic surfaces in boundary lubrication.

In contrast, when the aqueous solution of $EO_{19}PO_{29}EO_{19}$ was confined between two hydrophobic surfaces, the copolymers formed thin layers adsorbed onto the surfaces. Shearing did not have a significant change in their phase behavior. These thin films are expected to prevent hydrophobic surfaces from wearing and therefore may act as a lubricant layer.

## ASSOCIATED CONTENT

### Supporting Information

Simulations of the phase behavior of $EO_{19}PO_{29}EO_{19}$ in aqueous solution are provided as Supporting Information document. This includes MesoDyn phase morphology of polymer solutions at three concentrations, time evolution of PO chains morphology and the order parameter as a function of the simulation time. This material is available free of charge via the Internet at http://pubs.acs.org.

## AUTHOR INFORMATION

### Corresponding Author

*E-mail: ojrojas@ncsu.edu (O.J.R.); melissa_pasquinelli@ncsu.edu (M.A.P.).

### Present Addresses

[‡]Department of Earth and Atmospheric Sciences, Cornell University, Ithaca, New York 14853, United States

[∥]School of Chemical Technology, Department of Forest Products Technology, Aalto University, FI-00076 Aalto, Espoo, Finland.

## ACKNOWLEDGMENTS

This work was partially supported by the National Textile Center under Grant C05-NS09. We thank Dr. Juan Hinestroza at Cornell University for helpful discussions.

## REFERENCES

(1) de Vocht, M. L.; Scholtmeijer, K.; van der Vegte, E. W.; de Vries, O. M. H.; Sonveaux, N.; Wösten, H. A. B.; Ruysschaert, J.-M.; Hadziioannou, G.; Wessels, J. G. H.; Robillard, G. T. *Biophys. J.* **1998**, *74*, 2059.

(2) Troughton, E. B.; Bain, C. D.; Whitesides, G. M.; Nuzzo, R. G.; Allara, D. L.; Porter, M. D. *Langmuir* **1988**, *4*, 365.

(3) Linse, P. *Colloids Surf., A* **1994**, *86*, 137.

(4) Liu, X.; Wu, D.; Turgman-Cohen, S.; Genzer, J.; Theyson, T. W.; Rojas, O. J. *Langmuir* **2010**.

(5) Wang, Y. Q.; Su, Y. L.; Ma, X. L.; Sun, Q.; Jiang, Z. Y. *J. Membr. Sci.* **2006**, *283*, 440.

(6) Vivarat Perrin, M. P.; Amiel, C.; Sebille, B. *Langmuir* **1994**, *10*, 3635.

(7) Foster, B.; Cosgrove, T.; Espidel, Y. *Langmuir* **2009**, *25*, 6767.

(8) Foster, B.; Cosgrove, T.; Hammouda, B. *Langmuir* **2009**, *25*, 6760.

(9) Bardi, G.; Tognini, P.; Ciofani, G.; Raffa, V.; Costa, M.; Pizzorusso, T. *Nanomed.: Nanotechnol., Biol. Med.* **2009**, *5*, 96.

(10) Linse, P. *Macromolecules* **1993**, *26*, 4437.

(11) Loiola, A. R.; Da Silva, L. R. D.; Cubillas, P.; Anderson, M. W. *J. Mater. Chem.* **2008**, *18*, 4985.

(12) Leventis, N.; Mulik, S.; Wang, X.; Dass, A.; Patil, V. U.; Sotiriou-Leventis, C.; Lu, H.; Churu, G.; Capecelatro, A. *J. Non-Cryst. Solids* **2008**, *354*, 632.

(13) Batrakova, E. V.; Kabanov, A. V. *J. Controlled Release* **2008**, *130*, 98.

(14) Yong, M. J. Q.; Wong, A. S. W.; Ho, G. W. *Mater. Chem. Phys.* **2009**, *116*, 563.

(15) Tien, C.-P.; Teng, H. *J. Taiwan Inst. Chem. Eng.* **2009**, *40*, 452.

(16) Stoychev, I.; Galy, J.; Fournel, B.; Lacroix-Desmazes, P.; Kleiner, M.; Sadowski, G. *J. Chem. Eng. Data* **2009**, *54*, 1551.

(17) Lazzara, G.; Milioto, S. *J. Phys. Chem. B* **2008**, *112*, 11887.

(18) Govender, S.; Swart, P. *Colloids Surf., A* **2008**, *331*, 97.

(19) Sakar-Deliormanli, A. *J. Eur. Ceramic Soc.* **2007**, *27*, 611.

(20) Galy, J.; Sawada, K.; Fournel, B.; Lacroix-Desmazes, P.; Lagerge, S.; Persin, M. *J. Supercrit. Fluids* **2007**, *42*, 69.

(21) Steitz, R.; Schemmel, S.; Hongwei, S.; Findenegg, G. H. *J. Phys.: Condens. Matter* **2005**, *17*, 665.

(22) Li, Y.; Hinestroza, J. Boundary lubircation phenomena in coated textile surfaces. In *Friction in Textile Materials*; Gupta, B. S., Ed.; Woodhead Publishing: Cambridge, U.K., 2007; pp 419.

(23) Song, J.; Liang, J.; Liu, X.; Krause, W. E.; Hinestroza, J. P.; Rojas, O. J. *Thin Solid Films* **2009**, *517*, 4348.

(24) Brandani, P.; Stroeve, P. *Macromolecules* **2003**, *36*, 9492.

(25) Brandani, P.; Stroeve, P. *Macromolecules* **2003**, *36*, 9502.

(26) Brandani, P.; Stroeve, P. *Macromolecules* **2004**, *37*, 6640.

(27) Li, Y.; Liu, H.; Song, J.; Rojas, O. J.; Hinestroza, J. P. *ACS Appl. Mater. Interfaces* **2011**, *3*, 2349.

(28) Fraaije, J. G. E. M. *J. Chem. Phys.* **1993**, *99*, 9202.

(29) Alexandridis, P.; Olsson, U.; Lindman, B. *Macromolecules* **1995**, *28*, 7700.

(30) Zvelindovsky, A. V.; Sevink, G. J. A.; van Vlimmeren, B. A. C.; Maurits, N. M.; Fraaije, J. G. E. M. *Phys. Rev. E* **1998**, *57*, 4879.

(31) van Vlimmeren, B. A. C.; Maurits, N. M.; Zvelindovsky, A. V.; Sevink, G. J. A.; Fraaije, J. G. E. M. *Macromolecules* **1999**, *32*, 646.

(32) Fraaije, J. G. E. M.; Zvelindovsky, A. V.; Sevink, G. J. A.; Maurits, N. M. *Mol. Simulat.* **2000**, *25*, 131.

(33) Nicolaides, D. *Mol. Simul.* **2001**, *26*, 51.

(34) Lam, Y.-M.; Goldbeck-Wood, G. *Polymer* **2003**, *44*, 3593.

(35) Fraaije, J. G. E. M.; Zvelindovsky, A. V.; Sevink, G. J. A. *Mol. Simul.* **2004**, *30*, 225.

(36) Fraaije, J. G. E. M.; Van Vlimmeren, B. A. C.; Maurits, N. M.; Postma, M.; Evers, O. A.; Hoffmann, C.; Altevogt, P.; Goldbeck-Wood, G. *J. Chem. Phys.* **1997**, *106*, 4260.

(37) Spyriouni, T.; Vergelati, C. *Macromolecules* **2001**, *34*, 5306.

(38) Jawalkar, S. S.; Adoor, S. G.; Sairam, M.; Nadagouda, M. N.; Aminabhavi, T. M. *J. Phys. Chem. B* **2005**, *109*, 15611.

(39) Jawalkar, S. S.; Nataraj, S. K.; Raghu, A. V.; Aminabhavi, T. M. *J. Appl. Polym. Sci.* **2008**, *108*, 3572.

(40) Yang, S.; Yuan, S.; Zhang, X.; Yan, Y. *Colloids Surf. A* **2008**, *322*, 87.

(41) Zhang, X.; Yuan, S.; Wu, J. *Macromolecules* **2006**, *39*, 6631.
(42) Knoll, A.; Horvat, A.; Lyakhova, K. S.; Krausch, G.; Sevink, G. J. A.; Zvelindovsky, A. V.; Magerle, R. *Phys. Rev. Lett.* **2002**, *89*, 035501.
(43) Knoll, A.; Magerle, R.; Krausch, G. *J. Chem. Phys.* **2004**, *120*, 1105.
(44) Horvat, A.; Lyakhova, K. S.; Sevink, G. J. A.; Zvelindovsky, A. V.; Magerle, R. *J. Chem. Phys.* **2004**, *120*, 1117.
(45) Lyakhova, K. S.; Horvat, A.; Zvelindovsky, A. V.; Sevink, G. J. A. *Langmuir* **2006**, *22*, 5848.
(46) *Accelrys. Materials Studio*; Accelrys Software: San Diego, 2001−2010.
(47) Li, Y.; Hou, T.; Guo, S.; Wang, K.; Xu, X. *Phys. Chem. Chem. Phys.* **2000**, *2*, 2749.
(48) Flory, P. J. *Principles of Polymer Chemistry*; Cornell University Press: Ithaca, NY, 1953.
(49) Guo, S. L.; Hou, T. J.; Xu, X. J. *J. Phys. Chem. B* **2002**, *106*, 11397.
(50) Zhao, Y.; Chen, X.; Yang, C.; Zhang, G. *J. Phys. Chem. B* **2007**, *111*, 13937.
(51) Alexandridis, P.; Holzwarth, J. F.; Hatton, T. A. *Macromolecules* **1994**, *27*, 2414.
(52) Liu, H. *Fiber Lubrication: A Molecular Dynamics Simulation Study*. PhD Thesis, North Carolina State University, Raleigh, NC, 2009.
(53) Maurits, N. M.; van Vlimmeren, B. A. C.; Fraaije, J. G. E. M. *Phys. Rev. E* **1997**, *56*, 816.